

Article

Fe₃ Cluster Anchored on the C₂N Monolayer for Efficient Electrochemical Nitrogen Fixation

Bing Han ¹, Haihong Meng ¹, Fengyu Li ^{1,*} and Jingxiang Zhao ^{2,*}

¹ Physical School of Science and Technology, Inner Mongolia University, Hohhot 010021, China; binghan1214@163.com (B.H.); dundun_0521@163.com (H.M.)

² College of Chemistry and Chemical Engineering, Key Laboratory of Photonic and Electronic Bandgap Materials, Ministry of Education, Harbin Normal University, Harbin 150025, China

* Correspondence: fengyuli@imu.edu.cn (F.L.); zhaojingxiang@hrbnu.edu.cn (J.Z.)

Received: 27 July 2020; Accepted: 22 August 2020; Published: 29 August 2020



Abstract: Under the current double challenge of energy and the environment, an effective nitrogen reduction reaction (NRR) has become a very urgent need. However, the largest production of ammonia gas today is carried out by the Haber–Bosch process, which has many disadvantages, among which energy consumption and air pollution are typical. As the best alternative procedure, electrochemistry has received extensive attention. In this paper, a catalyst loaded with Fe₃ clusters on the two-dimensional material C₂N (Fe₃@C₂N) is proposed to achieve effective electrochemical NRR, and our first-principles calculations reveal that the stable Fe₃@C₂N exhibits excellent catalytic performance for electrochemical nitrogen fixation with a limiting potential of 0.57 eV, while also suppressing the major competing hydrogen evolution reaction. Our findings will open a new door for the development of non-precious single-cluster catalysts for effective nitrogen reduction reactions.

Keywords: C₂N-supported Fe₃ catalyst; nitrogen reduction reaction (NRR); density functional theory (DFT)

1. Introduction

Ammonia (NH₃) is an important chemical in agriculture and industry [1], and the direct reduction of nitrogen to ammonia is still considered to be one of the most important and challenging chemical transformations [2]. Dinitrogen (N₂), as the component with the largest volume fraction (78.08%) in the Earth's atmosphere, is the main source of nitrogen [3]. Therefore, ammonia can be directly synthesized from the Earth's abundant nitrogen resources. Usually, the Haber–Bosch process (N₂ + 3H₂ = 2NH₃) is used to synthesize ammonia on large scales. In this process, iron and ruthenium-based metal catalysts are used to convert atmospheric nitrogen (N₂) into NH₃ by reacting with hydrogen (H₂) [4,5]; the adsorbed N₂ molecule is firstly dissociated on specific active sites of the catalysts [6–8], and then the dissociated N species are hydrogenated, which is known as the dissociation mechanism [9]. However, extreme reaction conditions are usually required, such as high pressure (~100 bar) and high temperature (~700 K) [10]; as the reaction proceeds, a large amount of carbon dioxide is emitted, and the energy consumed each year is huge. On the other hand, the conditions of high temperature and pressure may not be necessary because the reaction is actually exothermic [10]. For this reason, it is of significance to search for a green and cost-effective method for the production of ammonia [11].

With continuous efforts, scientists have found that the electrochemical nitrogen reduction reaction (NRR, N₂ + 6H⁺ + 6e⁻ = 2NH₃) [12] under environmental conditions is extremely attractive because of its greatly reduced energy input and good environmental compatibility. Here, the electrocatalyst is the core component for reducing the reaction limit potential and increasing the reaction speed and the selectivity of NH₃ [13]. For NRR, one of the key challenges is the activation of nitrogen, which is

due to the highly stable $\text{N}\equiv\text{N}$ bond [14]. The capability of N_2 adsorption strongly depends on the electronic structure of the elements in the catalysts, since only the elements possess unoccupied d orbitals; d orbitals with an appropriate symmetry can accept the electrons of N_2 , and the occupied d orbitals of these elements can back donate to the π orbitals of N_2 , thus weakening the $\text{N}\equiv\text{N}$ bond [15]. Suitable and active catalysts can break the $\text{N}\equiv\text{N}$ bond, and hence, the single nitrogen atoms react with hydrogen to form ammonia. In recent years, not only single-atom catalysts (SACs) [12–21] have been emerging as a novel strategy for designing effective electrocatalysts for NRR: the catalytic performance of double atomic catalysts (DACs) [21–24] and triple atomic catalysts (TACs) [25,26] for NRR has also been explored both experimentally and theoretically.

Many transition-metal (TM) species, such as Fe, Ru, Co and Mo-based complexes, have been used for nitrogen fixation, because the occupied d orbitals of these metals can donate electrons to the empty π^* -orbital of N_2 and accept electrons from its σ -orbital, thereby enhancing the adsorption of N_2 [23]. Among the transition metals, Mo and Fe were considered to be the most promising metal species because, based on density functional theory (DFT) calculations, Mo and Fe were located at the top of the volcano map [27], and Fe has received the most attention because of its robustness and low cost [16]. For example, in 2018, Li's group proposed that $\text{Fe}_3@ \text{Al}_2\text{O}_3$ as a catalyst for NRR has superior catalytic performance [25], and quite recently, Jiang and co-workers' DFT studies showed that the Fe_3 cluster loaded on a heterostructure of graphdiyne and graphene (GDY/Gra) also had excellent NRR catalytic activity [28]. Thus, we conceived that the Fe_3 clusters should have capable catalytic performance when supported on a suitable substrate, such as the C_2N monolayer. The C_2N monolayer was first fabricated in 2015 [22] and has a unique porous structure originating from a 2D graphene layer, which provides an ideal support for metal atoms as the active center and has a high surface-to-volume ratio property that ensures sufficient exposure of TM atoms to interact with reactant molecules [29]. Thus, we explored the stability of Fe_3 clusters anchored on the C_2N monolayer ($\text{Fe}_3@ \text{C}_2\text{N}$) and the electrocatalysis of NRR by means of density functional theory (DFT) computations. Our calculations show that $\text{Fe}_3@ \text{C}_2\text{N}$ is a stable metal and has excellent catalytic performance for the N_2 reduction reaction with the supported Fe_3 cluster serving as the active center.

2. Results and Discussion

2.1. The Geometry, Stability and Electronic Properties of the $\text{Fe}_3@ \text{C}_2\text{N}$

Two-dimensional (2D) C_2N is a porous material similar to graphene, and the hexagonal lattice parameter of the C_2N unit cell was calculated to be 8.32 Å, which matches well with previous studies [29]. The optimized geometric structure of C_2N is given in Figure 1a. In the C_2N monolayer, the C_6 rings are connected by N atoms, resulting in a six-membered nitrogen pore with a para-N distance of 5.51 Å; the pores provide desired sites to anchor metal atoms or clusters. Previous theoretical studies [30,31] showed that adding the second Fe atom to $\text{Fe}_1@ \text{C}_2\text{N}$ is energetically favored: the binding energy of the second Fe atom is comparable to that of the first one, and $\text{Fe}_2@ \text{C}_2\text{N}$ maintains its original structure throughout a 10 ps molecular dynamics simulation at 800 K [30]. Based on the porous structural feature in the C_2N monolayer and the stable $\text{Fe}_2@ \text{C}_2\text{N}$ complex [30,31], we conjectured that adding one more Fe atom to $\text{Fe}_2@ \text{C}_2\text{N}$, i.e., $\text{Fe}_3@ \text{C}_2\text{N}$, may also have good thermodynamic and thermal stability. According to our computations, the lowest-energy supported Fe_3 cluster adopts a buckled triangle structure, with each Fe bonded to two N atoms, and the buckling height of the Fe_3 structure is 1.29 Å, while the C_2N support almost maintains its flat configuration (Figure 1b), similar to the model proposed by Pei et al. [32]. The Fe–Fe and Fe–N bond lengths are in the range of 2.28–2.32 Å (slightly shorter than the 2.48 Å in the bulk phase) and 1.97–2.01 Å, respectively. The average binding energy per Fe atom is –4.12 eV, which is slightly lower than the value of –4.84 eV per Fe atom in the bulk phase at the same level of theory, indicating the good thermodynamic stability of $\text{Fe}_3@ \text{C}_2\text{N}$. Furthermore, a first-principles molecular dynamics (FPMD) simulation in an NVT ensemble with the temperature controlled by the Nosé–Hoover method [33] was performed, and the structure of

$\text{Fe}_3\text{@C}_2\text{N}$ was well kept through a 10 ps FPMD with a time step of 0.5 fs at 800 K (Figure S1). Thus, $\text{Fe}_3\text{@C}_2\text{N}$ is extraordinarily stable.

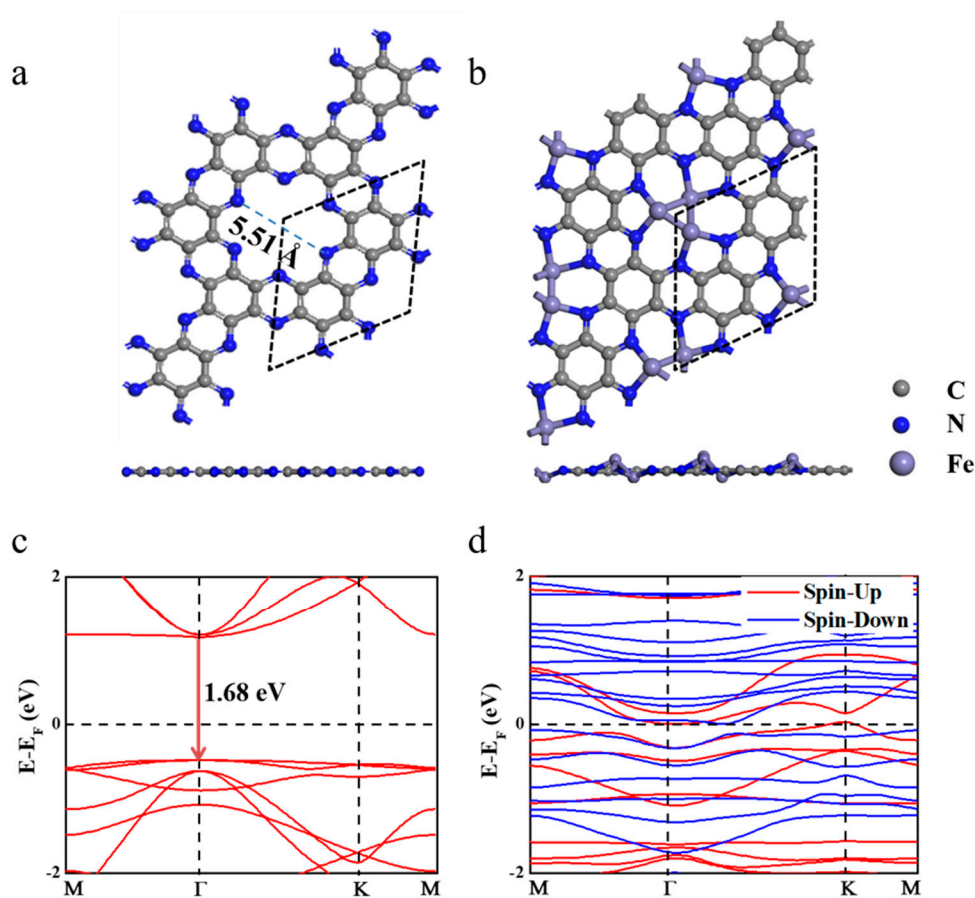


Figure 1. Top and side views of C_2N (a) and $\text{Fe}_3\text{@C}_2\text{N}$ (b), as well as their corresponding band structures (c,d).

Good electrical conductivity is required for fast charge transfer during efficient electrocatalytic processes. Compared to the semiconducting C_2N monolayer, whose band gap was calculated to be 1.68 eV (Figure 1c), in line with a previous report [29], $\text{Fe}_3\text{@C}_2\text{N}$ is a ferromagnetic (each Fe atom carries the magnetic moment of $\sim 3 \mu_{\text{B}}$, Figure S2) metal (Figure 1d), and the metallic feature originates from the states that have crossed the Fermi level, which is dominantly attributed to the Fe-d orbitals (Figure S3). The charge transfer between the Fe_3 cluster and C_2N is 2.12 $|e|$, indicating the high activity of the Fe_3 cluster.

2.2. N_2 Adsorption on $\text{Fe}_3\text{@C}_2\text{N}$

Previous investigations proposed the following criteria for an efficient electrocatalyst for NRR: (1) the catalyst can facilitate the chemisorption of N_2 molecules to sufficiently activate the inert $\text{N}\equiv\text{N}$ triple bonds, and (2) the catalyst can selectively stabilize N_2H^* and (3) destabilize NH_2^* species to lower the limiting potential [12]. In the electrochemical synthesis of ammonia, the adsorption of nitrogen is considered to be the first step, and the initial nitrogen adsorption configuration plays an important role in subsequent reactions [9]. On pristine C_2N , the adsorption of N_2 is very weak, and the adsorption energy (E_{ads}) is only -0.01 eV, which indicates that the pristine C_2N monolayer cannot effectively activate nitrogen. Zhao's theoretical group also found that N_2 adsorption on C and N atoms is rather weak ($E_{\text{ads}} < -0.20$ eV), or the N_2 molecule is spontaneously trapped by the central TM atoms after structural optimization on $\text{TM@C}_2\text{N}$ [34]. In our work, we considered two adsorption configurations,

namely, end-on and side-on structures of N_2 on the Fe_3 cluster anchored on C_2N (Figure 2), and the adsorption energies of the two configurations are -1.08 and -1.45 eV, respectively. The E_{ads} values are sufficiently strong to capture and activate N_2 , as indicated by the elongated $N\equiv N$ lengths of 1.16 and 1.26 Å (the isolated $N\equiv N$ length was calculated to be 1.11 Å) and a charge transfer of -0.57 and -1.14 |e| for the end-on and side-on configurations, respectively. Compared to the maximum vibrational frequency of free N_2 (2420 cm^{-1}), the maximum vibrational mode of the adsorbed N-N in the side-on (end-on) configuration is 1380 (2011) cm^{-1} . The remarkably reduced frequency in the side-on structure suggests an apparent elongation/weakening in the N-N bond upon N_2 being adsorbed on $Fe_3@C_2N$.

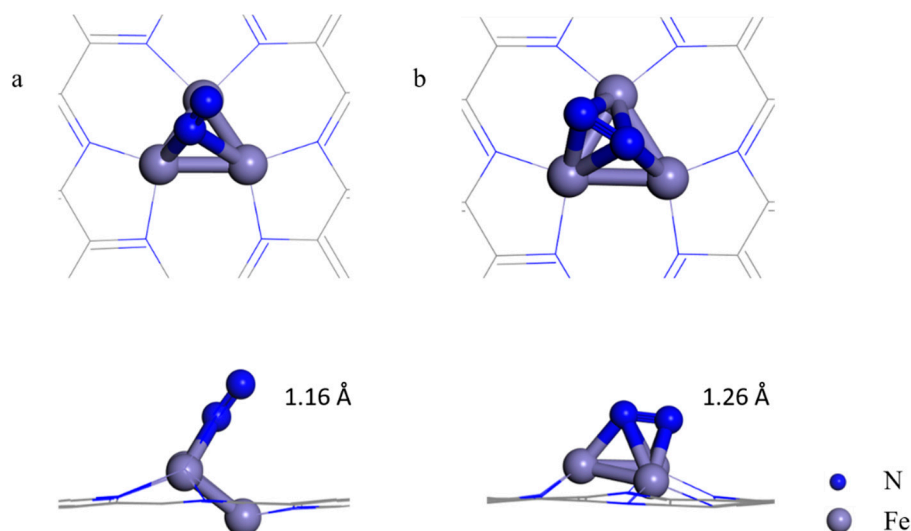


Figure 2. Top and side views of N_2 adsorbed on the $Fe_3@C_2N$ with the end-on (a) and side-on configuration (b).

2.3. N_2 Reaction on $Fe_3@C_2N$

Considering the energetically preferred side-on configuration and the greater charge transfer between N_2 and $Fe_3@C_2N$, as well as the much longer stretched $N\equiv N$ length, we selected the N_2 adsorption with the side-on structure as the starting state for NRR.

Previous studies revealed that the N_2 molecule could dissociate directly on the specific iron surface, such as Fe(111) and Fe(211) surfaces [35,36]; we first examined the dissociative mechanism. However, our computations showed that the dissociated NN state on $Fe_3@C_2N$ is not energetically favored, since it is 2.67 eV higher in energy than the N_2 adsorbed state (Figure S4), suggesting a very high activation energy barrier (>2.67 eV) of N_2 dissociation. For comparison, the calculated barrier of N_2 dissociation is as high as 1.89 eV on $Fe_3/\theta-Al_2O_3(010)$ [25]. Thus, the dissociative mechanism of NRR over $Fe_3@C_2N$ was not further studied in our work. Quite recently, Wang's theoretical group proposed a new mechanism for NRR, namely, a surface-hydrogenation mechanism [37], where the surface hydrogenation can drive the N_2 reduction reaction. We also tested the surface-hydrogenation mechanism of NRR on $Fe_3@C_2N$; nevertheless, N_2 adsorption on the hydrogenated Fe_3 cluster is endothermic at 2.41 eV (Figure S5), indicating an unfavorable pathway for NRR. Therefore, we focused on the associative mechanism in the following experiment.

For the associative mechanism, we compared the enzymatic ($* \rightarrow *N_2 \rightarrow *NNH \rightarrow *HNNH \rightarrow *HNNH_2 \rightarrow *H_2NNH_2 \rightarrow *H_3NNH_2 \rightarrow *NH_2 \rightarrow *NH_3 \rightarrow NH_3(g)$) and consecutive ($* \rightarrow *N_2 \rightarrow *NNH \rightarrow *NNH_2 \rightarrow *NNH_3 \rightarrow *N \rightarrow *NH \rightarrow *NH_2 \rightarrow *NH_3 \rightarrow NH_3(g)$) pathways [38] for NRR (Figure 3a), and the free energy change for each step is illustrated in Figure 3b,c. The difference between the two mechanisms is that in the enzymatic mechanism, the proton–electron pair ($H^+ + e^-$) alternately attacks two N atoms, while in the consecutive mechanism, the proton–electron pair first continuously approaches one N atom to generate the first NH_3 and then attacks the other N atom to generate the

second NH_3 [39]. The free energy difference for each elementary step in the enzymatic (consecutive) route is $-0.92, 0.28, -0.02, 0.57, -1.82, 0.11, 0.54, 0.44$ and 0.01 ($-0.92, 0.28, 0.83, -1.51, 0.28, -0.78, 0.57, 0.44$ and 0.01) eV, respectively, and accordingly, the potential limiting step $^*\text{HNNH} \rightarrow ^*\text{HNNH}_2$ ($^*\text{NNH} \rightarrow ^*\text{NNH}_2$) has a maximum free energy change of 0.57 (0.83) eV via the enzymatic (consecutive) mechanism. Thus, the limiting potential (η) of NRR on $\text{Fe}_3\text{@C}_2\text{N}$ is as low as -0.57 V, lower than the η values on the Ru (0001) step surface [40] and $\text{Fe}_2\text{@C}_2\text{N}$ [24] (0.98 eV and 1.23 eV, respectively). Typically, the potential limiting step on most metal surfaces (such as Re, Ru, Rh and Fe) or two-dimensional MBenes is either the first hydrogenation (forming $^*\text{NNH}$) or the last protonation ($^*\text{NH}_3$ formation or NH_3 desorption) [9,41]. However, on $\text{Fe}_3\text{@C}_2\text{N}$, the free energy change of $^*\text{N}_2 \rightarrow ^*\text{NNH}$ is only 0.28 eV. We also calculated the barriers of the potential limiting steps of the two mechanisms, and the barriers are both 1.11 eV based on the CI-NEB method (Figure S6), lower than the corresponding values (1.24 and 1.31 eV) on $\text{Fe}_3\text{@}\theta\text{-Al}_2\text{O}_3(010)$ [25]. All of the above results suggest the high activity of $\text{Fe}_3\text{@C}_2\text{N}$ for NRR.

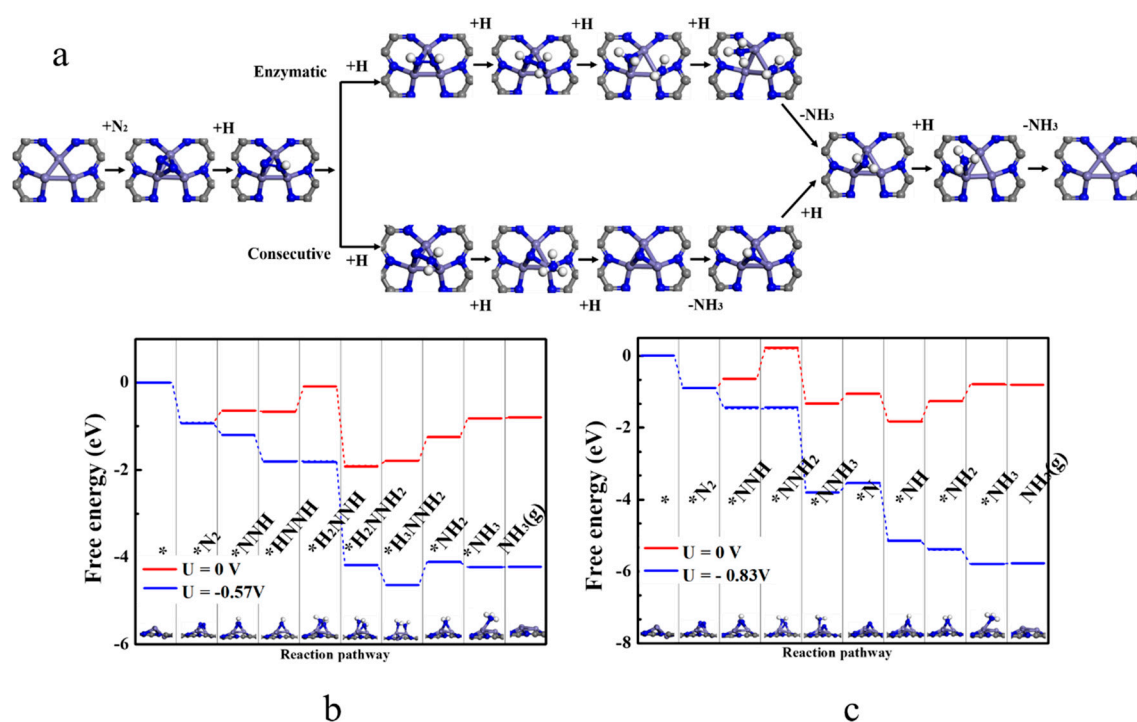


Figure 3. (a) Two nitrogen reduction reaction (NRR) pathways on $\text{Fe}_3\text{@C}_2\text{N}$, and the free energy diagram through enzymatic (b) and consecutive mechanisms (c) at different limiting potentials.

In addition to the catalytic activity, another important aspect for the catalytic performance is the selectivity of NRR [22]. Due to the high content of protons in the acidic solution, the major competitive reaction of NRR is the hydrogen evolution reaction (HER). The adsorption energy of $^*\text{H}$ on $\text{Fe}_3\text{@C}_2\text{N}$ is -0.94 eV, weaker than E_{ads} of N_2 (-1.45 eV), and expectedly, the charge transfer between $^*\text{H}$ and the catalyst is smaller ($0.43 |e|$ vs. $1.14 |e|$). By comparing the energies of two $^*\text{H}$ on $\text{Fe}_3\text{@C}_2\text{N}$ (-1.69 eV) and the formation of H_2 (1.79 eV, illustrated in Figure S7), we found that the reaction energy of HER is as high as 3.45 eV, indicating that $\text{Fe}_3\text{@C}_2\text{N}$ has a high ability to suppress the competing HER during NRR under an acidic environment. The stable and metallic $\text{Fe}_3\text{@C}_2\text{N}$ not only possesses low NRR limiting potential but also exhibits high selectivity against HER, and therefore, the low-cost $\text{Fe}_3\text{@C}_2\text{N}$ is a highly promising electrocatalyst for NRR.

3. Materials and Methods

The spin-polarized density functional theory (DFT) calculations were carried out using the Vienna *Ab initio* Simulation Package (VASP 5.4.4) [42]. The exchange–correlation functional was described by the Perdew, Burke, and Ernzerhof (PBE) parameterization of the generalized gradient approximation (GGA) [43]. The projector augmented-wave (PAW) potential [44] was employed, and an electron configuration of $3d^7 4s^1$ was adopted for Fe. According to our tests, we found that the system is ferromagnetic, with each Fe atom carrying a magnetic moment of $\sim 3 \mu_B$ (Figure S2), which is quite similar to the case of a Fe_3 cluster on the $\theta\text{-Al}_2\text{O}_3(010)$ surface [25]. A cutoff energy of 550 eV was adopted. The van der Waals interactions were described using the empirical correction in the Grimme scheme (DFT-D2) [45], where the dispersion energy is corrected based on the pairwise atomic $-C/R^6$ terms. The D2 scheme was widely used in these theoretical studies for the oxygen reduction reaction [29] and NRR [2]. During the structure relaxation, the maximum force and energy on each atom were less than 0.01 eV/\AA and 10^{-5} eV , the width of smearing was chosen as 0.2 eV, and k-points were sampled using the $5 \times 5 \times 1$ Monkhorst–Pack mesh [46]. To avoid the interaction between two neighboring surfaces, a vacuum space over 20 \AA was used [2,40]. To simulate a C_2N monolayer, a periodic 1×1 unit cell (with a lateral dimension of $\sim 8.34 \text{ \AA}$) containing 12 carbon atoms and 6 nitrogen atoms was constructed. The barriers of the potential limiting steps were identified by using the climbing image nudged elastic-band (CI-NEB) method [47].

The average binding energy (E_b) of each Fe atom on the C_2N substrate in our work is given by

$$E_b = (E_{Fe_3@C_2N} - E_{C_2N} - 3E_{Fe})/3$$

where $E_{Fe_3@C_2N}$, E_{C_2N} and E_{Fe} are the energies of the $Fe_3@C_2N$ system, the C_2N monolayer, and an isolated Fe atom, respectively.

The adsorption energy (E_{ads}) of the single atom or NRR intermediates was determined according to the following equation:

$$E_{ads} = E_{tot} - E_{Fe_3@C_2N} - E_{adsorbate}$$

where E_{tot} , $E_{Fe_3@C_2N}$ and $E_{adsorbate}$ represent the total energies of the systems containing the $Fe_3@C_2N$ catalyst and the adsorbate, $Fe_3@C_2N$, and the adsorbate, respectively.

According to the calculated hydrogen electrode (CHE) model proposed by Nørskov and co-workers [48], the reaction free energy of each basic step ΔG is calculated by

$$\Delta G = \Delta E - \Delta E_{ZPE} - T\Delta S + eU + \Delta G_{pH}$$

In the above equation, ΔE is the reaction energy difference between the products and reactants of the NRR occurring on the catalyst, which can be directly obtained from DFT computations, and ΔE_{ZPE} is the change in zero-point energies, which was calculated from the vibrational frequencies [12]. The vibrational frequencies were calculated based on the finite differences method, and only the adsorbed species were included. ΔS is the change in entropy at 298.15 K. Among them, the free energy correction of pH is expressed by ΔG_{pH} , which is equal to $k_B T \times \ln 10 \times \text{pH}$, where k_B is the Boltzmann constant. In this study, it is assumed that $\text{pH} = 0$.

The limiting potential (η) of the entire reduction process is determined by the potential limiting step, which has the most positive ΔG (ΔG_{Max}), as computed by $\eta = -\Delta G_{Max}/e$ [49].

The reaction rates of the key reaction steps were estimated based on Nørskov's model [48], provided that there is no extra barrier: $k = k_0 \exp(-\Delta G/k_B T)$, where ΔG is the free energy change and k_0 is the prefactor. The approximated values are given in Table S3.

4. Conclusions

In summary, we designed a supported catalyst, i.e., Fe_3 clusters anchored on a two-dimensional C_2N monolayer ($Fe_3@C_2N$), to electrocatalyze the reduction of nitrogen to ammonia. Through our

density functional theory computations, we found that $\text{Fe}_3\text{@C}_2\text{N}$ is excellent as an electrocatalyst for NRR owing to the stability at high temperature (800 K), the metallic feature, the absence of precious metal, the low limiting potential (0.57 eV of the enzymatic mechanism) and the high selectivity against the competing side reaction, HER. Such superiority can be ascribed to the partially occupied d orbitals and largely negative charged Fe_3 cluster, which is beneficial in activating the inert $\text{N}\equiv\text{N}$ triple bond. Since it was feasible to reach $\text{Cu}_2\text{@C}_2\text{N}$ using CuCl_2 as a metal precursor in a previous theoretical protocol [50], $\text{Fe}_3\text{@C}_2\text{N}$ could be synthesized using FeCl_2 and other proper iron precursors. We hope that our work can inspire more experimental and theoretical studies to further explore the potential of non-precious metal clusters for NRR.

Supplementary Materials: The following are available online at <http://www.mdpi.com/2073-4344/10/9/974/s1>: Figure S1: Top and side views of the final structure of $\text{Fe}_3\text{@C}_2\text{N}$ through a 10 ps FPMD simulation at 800 K; Figure S2: The magnesium distribution of $\text{Fe}_3\text{@C}_2\text{N}$; Figure S3: Density of states (DOS) of C_2N and $\text{Fe}_3\text{@C}_2\text{N}$; Figure S4: The energy diagram of N_2 dissociation on $\text{Fe}_3\text{@C}_2\text{N}$; Figure S5: The energy diagram of NRR via the surface-hydrogenation mechanism on $\text{Fe}_3\text{@C}_2\text{N}$; Figure S6: The reaction pathway of the potential limiting step of the enzymatic mechanism and the consecutive mechanism; Figure S7: The energy diagram of the hydrogen evolution reaction (HER0 on $\text{Fe}_3\text{@C}_2\text{N}$; Table S1: The calculated zero-point energy (ZPE) and entropy of different molecules ($T = 298.15$ K and $P = 101.325$ Pa, in eV); Table S2: The calculated E(DFT), ZPE and TS of the intermediates ($T = 298.15$ K and $P = 101.325$ Pa, in eV); Table S3: The estimated reaction rate of each step on different paths (k_0 is the prefactor of the estimated reaction rate $k = k_0\exp(-\Delta G/kT)$).

Author Contributions: F.L. and J.Z. outlined the work plan; B.H. and H.M. conducted the computations; B.H. drew the figures and drafted the manuscript. All authors participated in the reviewing and publication processes of the article. All authors have read and agreed to the published version of the manuscript.

Funding: This work was funded by the National Natural Science Foundation of China (11704203), the Startup Project of Inner Mongolia University (21200-5175101), and the Natural Science Funds for Distinguished Young Scholar of Heilongjiang Province (JC2018004).

Acknowledgments: The authors acknowledge the support of this study by the National Natural Science Foundation of China, under Grant number (11704203), the Startup Project of Inner Mongolia University (21200-5175101), and the Natural Science Funds for Distinguished Young Scholar of Heilongjiang Province, under Grant number (JC2018004). Additionally, computational support from PARATEAR is appreciated.

Conflicts of Interest: The authors declare no conflict of interest.

References

1. Guo, X.; Li, X.; Li, Y.; Yang, J.; Wan, X.; Chen, L.; Liu, J.; Liu, X.; Yu, R.; Zheng, L.; et al. Molecule template method for precise synthesis of Mo-based alloy clusters and electrocatalytic nitrogen reduction on partially reduced PtMo alloy oxide cluster. *Nano Energy* **2020**, *78*, 105211. [CrossRef]
2. Guo, X.; Gu, J.; Lin, S.; Zhang, S.; Chen, Z.; Huang, S. Tackling the activity and selectivity challenges of electrocatalysts toward the nitrogen reduction reaction via atomically dispersed biatom catalysts. *J. Am. Chem. Soc.* **2020**, *142*, 5709–5721. [CrossRef] [PubMed]
3. Chen, X.; Li, N.; Kong, Z.; Ong, W.-J.; Zhao, X. Photocatalytic fixation of nitrogen to ammonia: State-of-the-art advancements and future prospects. *Mater. Horiz.* **2018**, *5*, 9–27. [CrossRef]
4. Van der Ham, C.J.M.; Koper, M.T.; Hetterscheid, D.G. Challenges in reduction of dinitrogen by proton and electron transfer. *Chem. Soc. Rev.* **2014**, *43*, 5183–5191. [CrossRef]
5. Shipman, M.A.; Symes, M.D. Recent progress towards the electrosynthesis of ammonia from sustainable resources. *Catal. Today* **2017**, *286*, 57–68. [CrossRef]
6. Logadóttir, Á.; Nørskov, J.K. Ammonia synthesis over a Ru(0001) surface studied by density functional calculations. *J. Catal.* **2003**, *220*, 273–279. [CrossRef]
7. Ertl, G.; Lee, S.B.; Weiss, M. Kinetics of nitrogen adsorption on Fe(111). *Surf. Sci.* **1982**, *114*, 515–526. [CrossRef]
8. Montoya, J.H.; Tsai, C.; Vojvodic, A.; Nørskov, J.K. The challenge of electrochemical ammonia synthesis: A new perspective on the role of nitrogen scaling relations. *ChemSusChem* **2015**, *8*, 2180–2186. [CrossRef]
9. Zhao, J.; Zhao, J.X.; Cai, Q.H. Single transition metal atom embedded into a MoS_2 nanosheet as a promising catalyst for electrochemical ammonia synthesis. *Phys. Chem. Chem. Phys.* **2018**, *20*, 9248–9255. [CrossRef]

10. Li, Q.Y.; He, L.Z.; Sun, C.H.; Zhang, X.W. Computational study of MoN₂ monolayer as electrochemical catalysts for nitrogen reduction. *J. Phys. Chem. C* **2017**, *121*, 27563–27568. [[CrossRef](#)]
11. Li, M.; Huang, H.; Low, J.; Gao, C.; Long, R.; Xiong, Y. Recent progress on electrocatalyst and photocatalyst design for nitrogen reduction. *Small Methods* **2019**, *3*, 1800388. [[CrossRef](#)]
12. Zhao, J.; Chen, Z. Single Mo atom supported on defective boron nitride monolayer as an efficient electrocatalyst for nitrogen fixation: A computational study. *J. Am. Chem. Soc.* **2017**, *139*, 12480–12487. [[CrossRef](#)] [[PubMed](#)]
13. Chen, Z.; Zhao, J.X.; Cabrera, C.R.; Chen, Z.F. Computational screening of efficient single-atom catalysts based on graphitic carbon nitride (g-C₃N₄) for nitrogen electroreduction. *Small Methods* **2018**, *2*, 1800368.
14. Li, Q.; Liu, C.; Qiu, S.; Zhou, F.; He, L.; Zhang, X.; Sun, C. Exploration of iron borides as electrochemical catalysts for nitrogen reduction reaction. *J. Mater. Chem. A* **2019**, *7*, 21507–21513. [[CrossRef](#)]
15. Cheng, H.; Ding, L.-X.; Chen, G.-F.; Zhang, L.; Xue, J.; Wang, H. Molybdenum carbide nanodots enable efficient electrocatalytic nitrogen fixation under ambient conditions. *Adv. Mater.* **2018**, *30*, 1803694. [[CrossRef](#)]
16. Li, X.-F.; Li, Q.-K.; Cheng, J.; Liu, L.; Yan, Q.; Wu, Y.C.; Zhang, X.Z.; Wang, Z.-Y.; Qiu, Q.; Luo, Y. Conversion of dinitrogen to ammonia by FeN₃ embedded graphene. *J. Am. Chem. Soc.* **2016**, *138*, 8706–8709. [[CrossRef](#)]
17. Azofra, L.M.; Sun, C.; Cavallo, L.; MacFarlane, D.R. Feasibility of N₂ binding and reduction to ammonia on Fe-deposited MoS₂ 2D sheets: A DFT study. *Chem. Eur. J.* **2017**, *23*, 8275–8279. [[CrossRef](#)]
18. Ling, C.; Ouyang, Y.X.; Li, Q.; Bai, X.; Mao, X.; Du, A.; Wang, J.L. A general two-step strategy-based high-throughput screening of single atom catalysts for nitrogen fixation. *Small Methods* **2018**, *3*, 1800376. [[CrossRef](#)]
19. Li, Q.; Qiu, S.; Liu, C.; Liu, M.; He, L.; Zhang, X.; Sun, C. Computational design of single molybdenum catalysts for nitrogen reduction reaction. *J. Phys. Chem. C* **2019**, *123*, 2347–2352. [[CrossRef](#)]
20. Wang, M.; Liu, S.; Qian, T.; Liu, J.; Zhou, J.; Ji, H.; Xiong, J.; Zhong, J.; Yan, C. Over 56.55% faradaic efficiency of ambient ammonia synthesis enabled by positively shifting the reaction potential. *Nat. Commun.* **2019**, *10*, 341. [[CrossRef](#)]
21. Liu, C.; Li, Q.; Zhang, J.; Jin, Y.; MacFarlane, D.R.; Sun, C. Conversion of dinitrogen to ammonia on Ru atoms supported on boron sheets: A DFT study. *J. Mater. Chem. A* **2019**, *7*, 4771–4776. [[CrossRef](#)]
22. Chen, Z.; Yan, J.; Jiang, Q. Single or double: Which is the altar of atomic catalysts for nitrogen reduction reaction? *Small Methods* **2018**, *3*, 1800291. [[CrossRef](#)]
23. Li, F.; Chen, L.; Liu, H.; Wang, D.; Shi, C.; Pan, H. Enhanced N₂-fixation by engineering the edges of two-dimensional transition-metal disulfides. *J. Phys. Chem. C* **2019**, *123*, 22221–22227. [[CrossRef](#)]
24. Zhang, X.; Chen, A.; Zhang, Z.H.; Zhou, Z. Double-atom catalysts: Transition metal dimer anchored C₂N monolayers as N₂ fixation electrocatalysts. *J. Mater. Chem. A* **2018**, *6*, 18599–18604. [[CrossRef](#)]
25. Liu, J.; Ma, X.; Li, Y.; Wang, Y.; Xiao, H.; Li, J. Heterogeneous Fe₃ single-cluster catalyst for ammonia synthesis via an associative mechanism. *Nat. Commun.* **2018**, *9*, 1610. [[CrossRef](#)] [[PubMed](#)]
26. Ma, D.W.; Zeng, Z.; Liu, L.; Huang, X.; Jia, Y. Computational evaluation of electrocatalytic nitrogen reduction on TM single-, double-, and triple-atom catalysts (TM = Mn, Fe, Co, Ni) based on graphdiyne monolayers. *J. Phys. Chem. C* **2019**, *123*, 19066–19076. [[CrossRef](#)]
27. Li, Y.; Zhang, Q.; Fan, H.-N.; Luo, W.-B.; Liu, H.-K.; Dou, S.-X. Atomically dispersed metal dimer species with selective catalytic activity for nitrogen electrochemical reduction. *J. Mater. Chem. A* **2019**, *7*, 22242–22247. [[CrossRef](#)]
28. Chen, Z.; Chen, L.; Jiang, M.; Chen, D.; Wang, Z.; Yao, X.; Singh, C.V.; Jiang, Q. Triple atom catalyst with ultrahigh loading potential for nitrogen electrochemical reduction. *J. Mater. Chem. A* **2020**, *8*, 15086–15093. [[CrossRef](#)]
29. Li, X.; Zhong, W.; Cui, P.; Li, J.; Jiang, J. Design of efficient catalysts with double transition metal atoms on C₂N layer. *J. Phys. Chem. Lett.* **2016**, *7*, 1750–1755. [[CrossRef](#)]
30. Zhang, X.; Chen, A.; Zhang, Z.H.; Jiao, M.G.; Zhou, Z. Transition metal anchored C₂N monolayers as efficient bifunctional electrocatalysts for hydrogen and oxygen evolution reactions. *J. Mater. Chem. A* **2018**, *6*, 11446–11452. [[CrossRef](#)]
31. Li, F.; Liu, X.; Chen, Z. 1 + 1' > 2: Heteronuclear biatom catalyst outperforms its homonuclear counterparts for CO oxidation. *Small Methods* **2019**, *10*, 1800480. [[CrossRef](#)]
32. Pei, W.; Zhou, S.; Zhao, J.; Xu, X.; Du, Y.; Dou, S.X. Immobilized trimeric metal clusters: A family of the smallest catalysts for selective CO₂ reduction toward multi-carbon products. *Nano Energy* **2020**, *76*, 105049. [[CrossRef](#)]

33. Martyna, G.J.; Klein, M.L.; Tuckerman, M. Nosè-Hoover chains: The canonical ensemble via continuous dynamics. *J. Chem. Phys.* **1992**, *97*, 2635–2643. [[CrossRef](#)]
34. Wang, Z.; Yu, Z.; Zhao, J. Computational screening of single transition metal atom supported on C₂N monolayer for electrochemical ammonia synthesis. *Phys. Chem. Chem. Phys.* **2018**, *20*, 12835–12844. [[CrossRef](#)] [[PubMed](#)]
35. Strongin, D.; Carrazza, J.; Bare, S.R.; Somorjai, G. The importance of C7 sites and surface roughness in the ammonia synthesis reaction over iron. *J. Catal.* **1987**, *103*, 213–215. [[CrossRef](#)]
36. Somorjai, G.; Materer, N. Surface structures in ammonia synthesis. *Top. Catal.* **1994**, *1*, 215–231. [[CrossRef](#)]
37. Ling, C.; Zhang, Y.; Li, Q.; Bai, X.; Shi, J.; Wang, J. New mechanism for N₂ reduction: The essential role of surface hydrogenation. *J. Am. Chem. Soc.* **2019**, *141*, 18264–18270. [[CrossRef](#)]
38. Gao, Z.; Huang, H.; Xu, S.; Li, L.; Yan, G.; Zhao, M.; Yang, W.; Zhao, X. Regulating the coordination environment through doping N atoms for single-atom Mn electrocatalyst of N₂ reduction with high catalytic activity and selectivity: A theoretical study. *Mol. Catal.* **2020**, *493*, 111091. [[CrossRef](#)]
39. Ling, C.; Bai, X.; Ouyang, Y.; Du, A.; Wang, J. Single molybdenum atom anchored on N-doped carbon as a promising electrocatalyst for nitrogen reduction into ammonia at ambient conditions. *J. Phys. Chem. C* **2018**, *122*, 16842–16847. [[CrossRef](#)]
40. Choi, C.; Back, S.; Kim, N.Y.; Lim, J.; Kim, Y.H.; Jung, Y. Suppression of hydrogen evolution reaction in electrochemical N₂ reduction using single-atom catalysts: A computational guideline. *ACS Catal.* **2018**, *8*, 7517–7525. [[CrossRef](#)]
41. Yang, X.; Shang, C.; Zhou, S.; Zhao, J. MBenes: Emerging 2D materials as efficient electrocatalysts for the nitrogen reduction reaction. *Nanoscale Horiz.* **2020**, *5*, 1106–1115. [[CrossRef](#)] [[PubMed](#)]
42. Kresse, G.; Furthmüller, F. Efficient iterative schemes for ab initio total-energy calculations using a plane-wave basis set. *Phys. Rev. B* **1996**, *54*, 11169–11186. [[CrossRef](#)] [[PubMed](#)]
43. Perdew, J.P.; Burke, K.; Ernzerhof, M. Generalized gradient approximation made simple. *Phys. Rev. Lett.* **1996**, *77*, 3865–3868. [[CrossRef](#)] [[PubMed](#)]
44. Blöchl, P.E. Projector augmented-wave method. *Phys. Rev. B* **1994**, *50*, 17953–17979. [[CrossRef](#)] [[PubMed](#)]
45. Bucko, T.; Hafner, J.; Lebegue, S.; Aangyan, J.G. Improved description of the structure of molecular and layered crystals: Ab initio DFT calculations with van der Waals Corrections. *J. Phys. Chem. A* **2010**, *114*, 11814–11824. [[CrossRef](#)] [[PubMed](#)]
46. Monkhorst, H.J.; Pack, D.J. Special points for Brillouin-zone integrations. *Phys. Rev. B* **1976**, *13*, 5188–5192. [[CrossRef](#)]
47. Henkelman, G.; Uberuaga, B.P.; Jónsson, H. A climbing image nudged elastic band method for finding saddle points and minimum energy paths. *J. Chem. Phys.* **2000**, *113*, 9901. [[CrossRef](#)]
48. Nørskov, J.K.; Rossmeisl, J.; Logadottir, A.; Lindqvist, L.; Kitchin, J.R.; Bligaard, T.; Jónsson, H. Origin of the overpotential for oxygen reduction at a fuel-cell cathode. *J. Phys. Chem. B* **2004**, *108*, 17886–17892. [[CrossRef](#)]
49. Skulason, E.; Bligaard, T.; Gudmundsdottir, S.; Studt, F.; Rossmeisl, J.; Abild-Pedersen, F.; Vegge, T.; Jónsson, H.; Nørskov, J.K. A theoretical evaluation of possible transition metal electro-catalysts for N₂ reduction. *Phys. Chem. Chem. Phys.* **2012**, *14*, 1235–1245. [[CrossRef](#)]
50. Li, F.; Chen, Z. Cu dimer anchored C₂N monolayer: Low-cost and efficient catalyst for CO oxidation. *Nanoscale* **2018**, *10*, 15696–15705. [[CrossRef](#)]

